www.czasopisma.pan.pl PAN POLSKA AKADEMIA NAUK www.journals.pan.pl

Arch. Metall. Mater. **64** (2019), 2, 579-583

DOI: 10.24425/amm.2019.127581

EUN-JEONG YI*, KEUN-YOUNG YOON*, HYUN-AH JUNG*, HAEJIN HWANG*#

# STABILITY OF GARNET-TYPE $Li_7La_3Zr_2O_{12}$-BASED CERAMICS FOR ALL-SOLID-STATE BATTERIES

Al and Nb-doped $Li_7La_3Zr_2O_{12}$ (LLZO) and W-doped LLZO lithium ion conducting electrolyte samples were prepared and their $H_2O$ stability was investigated. The LLZO samples were exposed to 50% humidified air for 48 h. After $H_2O$ exposure, a cubic to tetragonal transformation occurred and acquired SEM images exhibited the presence of reaction phases at the grain boundaries of Al and Nb-LLZO. As a result, the lithium ion conductivity significantly decreased after $H_2O$ exposure. On the contrary, W-LLZO showed good stability against $H_2O$. Although the cubic to tetragonal transformation was also observed in $H_2O$-exposed W-LLZO, the decrease in lithium ion conductivity was found to be modest. No morphological changes of the W-LLZO samples were confirmed in the $H_2O$-exposed W-LLZO samples.

*Keywords:* All-solid-state batteries, solid electrolytes, garnet type ceramics, ionic conductivity

## Introduction

Lithium-ion battery technology has advanced significantly in the last decade. However, future energy storage demands will require safer, cheaper and higher performance lithium batteries. Although the primary strategy for improving performance has focused on electrode materials [1-3], the development of lithium ion conducting solid electrolytes has attracted much attention as a potential opportunity to revolutionize lithium batteries [4,5]. Examples of technologies that could be facilitated by solid electrolytes include non-flammable solid-state lithium-ion batteries that do not require hermetic packaging, lithium-air fuel cells, and lithium-sulfur batteries.

Lithium ion conducting solid electrolytes can be divided into two categories of crystalline and amorphous. Lithium lanthanum titanate (LLTO) [6,7], sodium super ionic conductor (NASICON) – [8,9], thio-lithium super ionic conductor (LISICON) – [10] and garnet – [11,12] type Li-ion conductors are included in the crystalline category. On the other hand, oxides or sulfide glasses and LiPON are amorphous Li-ion conductors [13,14]. Among them, an oxide with the garnet structure ($Li_7La_3Zr_2O_{12}$, LLZO) exhibits high ionic conductivity ($4\times10^{-4}$ S·cm$^{-1}$ at room temperature), chemical stability against metallic lithium [15], and a large electrochemical potential window [16]. These excellent properties make LLZO a promising solid electrolyte material for all-solid-state batteries.

However, LLZO suffers from stability issues in ambient air which contains water vapor and carbon dioxide. Some researchers have concluded that a reaction between LLZO and air results in the observed decreased in lithium ion conductivity [17,18]. Liu et al. confirmed the formation of lithium carbonate ($Li_2CO_3$) after exposure to humid air and a reaction mechanism was proposed [19]. In addition, Jin et al. reported that a proton/$Li^+$ ion exchange reaction occurs between water and LLZO, leading to the decomposition of LLZO and a performance degradation [20].

In this study, we fabricated $Li_7La_3Zr_2O_{12}$ (LLZO)-based ceramics and symmetrical cells consisting of the LLZO electrolyte and platinum blocking electrodes. The LLZO samples were sintered under various atmospheres and subsequently exposed to humidified air. The effect of the sintering atmosphere and moisture exposure on the electrochemical performance of the LLZO electrolyte were investigated.

## 1. Experimental procedure

In this study, we prepared two types of electrolyte samples: Nb and Al co-doped $Li_7La_3Zr_2O_{12}$ (Al, Nb-LLZO) and W-doped $Li_{6.3}La_3Zr_{1.65}W_{0.35}O_{12}$ (W-LLZO). The Al, Nb-LLZO was fabricated by a conventional solid-state reaction process from lithium carbonate ($Li_2CO_3$, 98%, Junsei, Japan), lanthanum oxide ($La_2O_3$, 99.9%, GFS Chemicals, Japan), and zirconium oxide ($ZrO_2$, 99.0%, Samchun Pure Chemicals, Korea) powders. An appropriate amount of starting materials was mixed together using a planetary mill in ethyl alcohol (94.5%, Samchun Pure Chemicals, Korea) for 2 h in air. A 10 wt% excess $Li_2CO_3$ was added to compensate for lithium loss during high-temperature sintering. After drying, the powder mixtures were calcined at

* INHA UNIVERSITY, DEP. MATER. SCI. & ENG., 100 INHA-RO, MICHUHOL-GU, INCHEON 22212, KOREA

# Corresponding author: hjhwang@inha.ac.kr

900°C for 12 h. Subsequently, the calcined powders were pressed into pellet (20 mm-diameter disk), then sintered at 1200°C for 6 h. Prior to sintering, the LLZO powder compacts were isostatically pressed at 200 MPa.

For W-LLZO, commercially available powder was purchased from IFM ($Li_{6.3}La_3Zr_{1.65}W_{0.35}O_{12}$, Seoul, Korea). W-LLZO electrolyte samples were prepared using the same procedure as described in the preceding section. Sintered disk samples were polished using SiC papers in a dry atmosphere. The specimen size for characterization and electrochemical measurements was 15 mm diameter and 1 mm thickness.

Phase identification of sintered electrolyte samples was performed using X-ray diffraction (XRD, RU-200B, Rigaku Co., Ltd) with Ni-filtered CuKα radiation. The microstructure was examined by field emission scanning electron microscopy (FE-SEM, JSM-6700F, JEOL). The bulk density of the samples was determined using Archimedes' method. Lithium-ion conductivity was measured using an impedance analyzer (IM6e, Zahner). The AC impedance spectra were obtained under open circuit conditions with an excitation potential of 20 mV over the frequency range of 1 MHz to 0.01 Hz. Pt electrodes were incorporated in both sides of the electrolyte sample by a deposition process using dc-magnetron sputtering of a Pt target in Ar. Two Pt wires from the two electrodes were connected to the working and counter terminals of the impedance analyzer.

## 2. Results and discussion

In this study, LLZO powders were sintered at 1200°C for 6 h under air, $N_2$, and Ar atmospheres, and subsequently exposed to humidified (50% humidity) air for 48 h. Fig. 1 shows the XRD patterns of the Al and Nb-LLZO samples that were sintered in the different atmospheres and the Al and Nb-LLZO samples exposed to the humidified air. All the peaks of the as-sintered samples could be identified as being attributed to the cubic LLZO phase. There were no observed peaks ascribed to secondary phases or unreacted starting materials. On the contrary, the diffraction peaks which were attributed to a tetragonal type garnet structure were detected in the $H_2O$-exposed samples, particularly for the sample sintered in Ar. The stabilization of the cubic phase depends on the number of vacant lithium sites in the LLZO formula unit [11]. The possible reaction between LLZO and water vapor was responsible for the transformation from the cubic to tetragonal LLZO phase, although evidence of this is not observed in the XRD patterns of Fig. 1. Xia et al. reported on the formation of $La(OH)_3$ or $Li(OH)\cdot H_2O$ phases of the LLZO sample exposed to water vapor [20]. The observed discrepancy is due to the condition of the water vapor exposure.

Fig. 2 shows the AC impedance spectra of the as-sintered Al and Nb-LLZO samples and the LLZO samples exposed to humidified air. The impedance spectra exhibit a semicircle at high frequency followed by a spike at low frequency, which is often observed in symmetrical cells with blocking electrodes [21]. For the as-sintered samples, the semicircle corresponding to the bulk impedance is out with respect to the frequency scale of the instrumentation [11]. The impedance value increased significantly after the samples were exposed to the humidified air. The diameter of the impedance semicircle shown in Fig. 2 (a) and (b) corresponds to the resistance of the LLZO samples, and the conductivity of their lithium-ion is shown in Table 1. The conductivities of the as-sintered LLZO samples were from 3 to $4\times10^{-4}$ $S\cdot cm^{-1}$ regardless of the sintering atmosphere. This suggests that this factor did not affect the lithium ion conductivity of the Al and Nb-LLZO

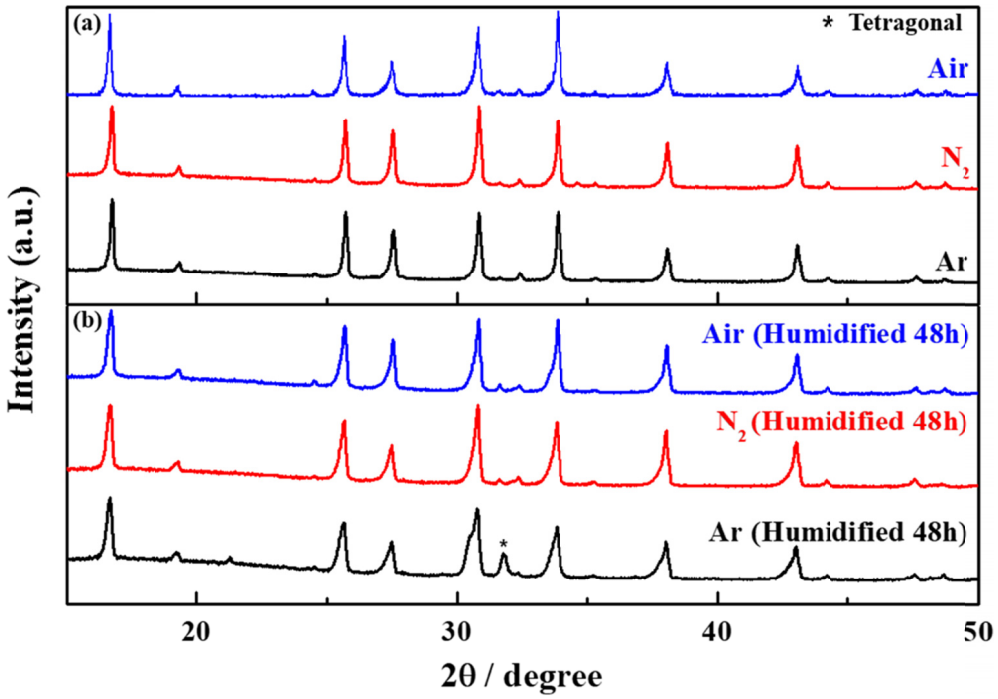


Fig. 1. XRD patterns of (a) as-sintered Al, Nb-LLZO and (b) $H_2O$-exposed LLZO samples. Air, $N_2$, and Ar indicate sintering atmospheres

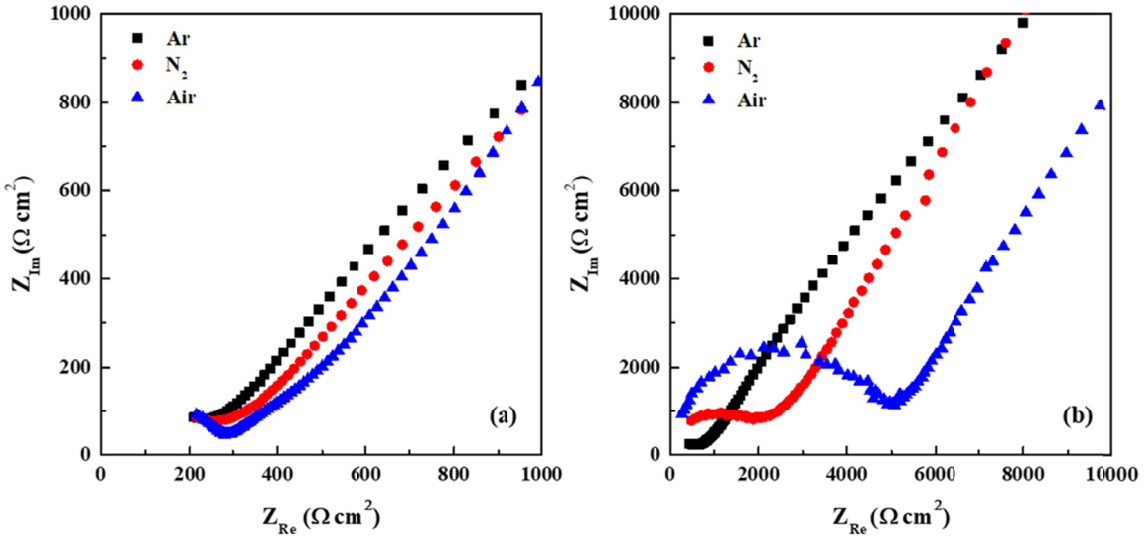


Fig. 2. AC impedance spectra of (a) as-sintered Al, Nb- LLZO and (b) $H_2O$-exposed LLZO samples. Air, $N_2$, and Ar indicate sintering atmospheres

samples. However, the conductivity decreased drastically after the water vapor exposure. This implies that the exposure results in a deterioration of the crystal structure or microstructure of Al and Nb-LLZO.

TABLE 1

Ionic conductivity of Al, Nb-LLZO and $H_2O$-exposed samples for 48 h

| Conductivity ($\times 10^{-4}$ S/cm) | Air | $N_2$ | Ar |
|---|---|---|---|
| As-prepared sample | 3.55 | 3.84 | 4.15 |
| $H_2O$-exposed sample | 0.197 | 0.535 | 1.75 |

SEM images of the as-sintered Al and Nb-LLZO and LLZO samples that were exposed to humidified air are shown in Fig. 3. A comparison of Fig. 3(b) with 3(a) indicates that a reaction phase (small particles) is formed in the LLZO grain boundaries, which is often observed in LLZO sample exposed to water vapor [19,20], although this is not detected in Fig. 1. The formation of a reaction phase can result in a decrease in lithium ion conductivity as shown in Table 1. In addition, tetragonal phase LLZO exhibits a lithium ion conductivity that is two orders of magnitude lower. This phase transformation from cubic to tetragonal can also contribute to the observed decreased conductivity.

Fig. 4 shows XRD patterns of the as-sintered W-LLZO and W-LLZO exposed to humidified air. Similar to the Al and Nb-LLZO sample, the as-sintered W-LLZO samples are cubic phase, while the tetragonal phase appears after $H_2O$ exposure. In the case of the W-LLZO sintered under an air environment and subsequently exposed to humidified air, the transformation to a tetragonal phase is distinct compared to the samples sintered

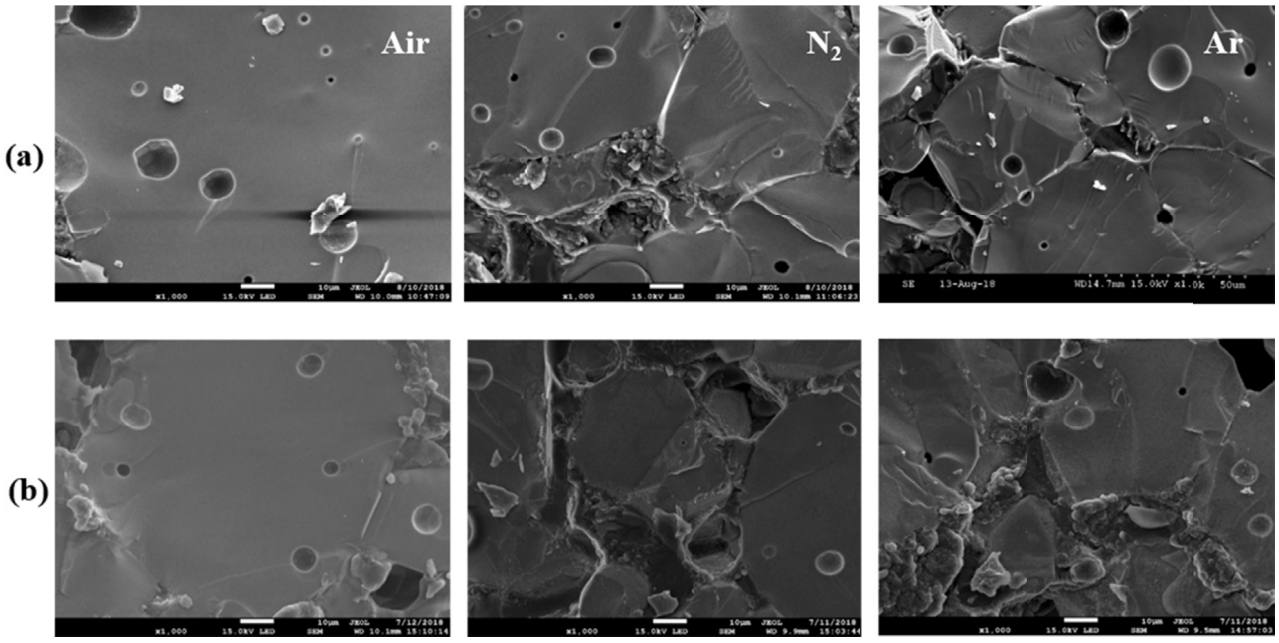


Fig. 3. SEM images of (a) as-sintered Al, Nb-LLZO and (b) $H_2O$-exposed LLZO samples. Air, $N_2$, and Ar indicate sintering atmospheres

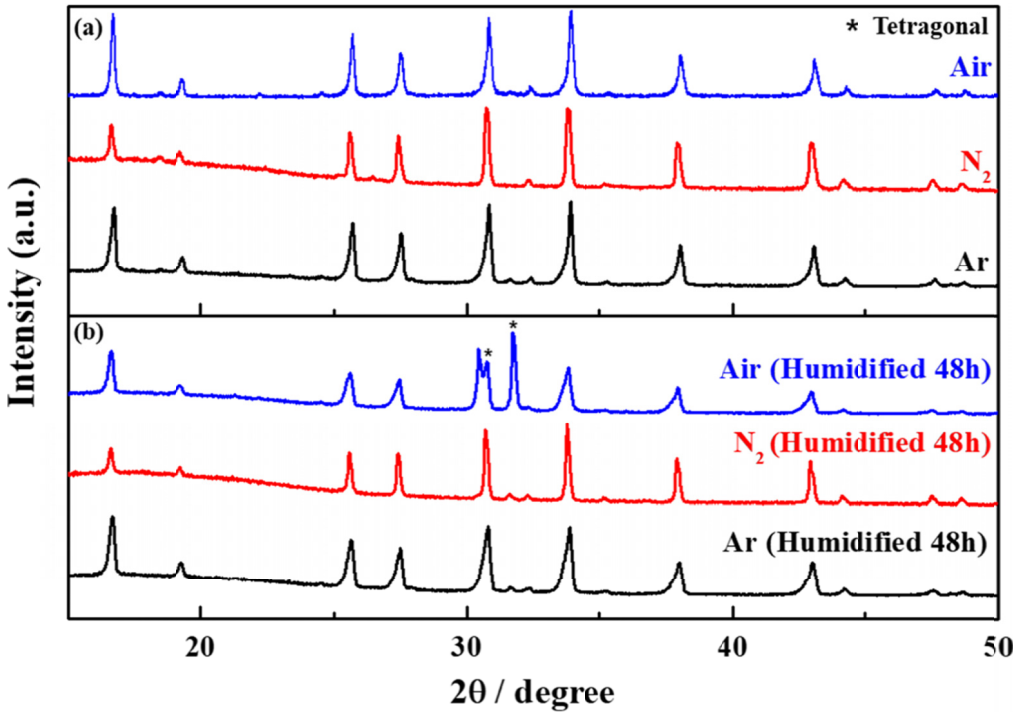


Fig. 4. XRD patterns of (a) as-sintered W-LLZO and (b) $H_2O$-exposed LLZO samples. Air, $N_2$, and Ar indicate sintering atmospheres

under $N_2$ and Ar environments. This observed phenomenon might be associated with the presence of impurities in humidified air. It appears that the tetragonal transformation does not lead to lithium ion conductivity of the W-LLZO samples. This phenomenon will be described in the following section.

Fig. 5 show the AC impedance spectra of as-sintered W-LLZO samples and W-LLZO samples exposed to humidified air. Although the impedance arcs of the $H_2O$-exposed W-LLZO samples are slightly larger than that of the as-sintered W-LLZO samples, the shape of the impedance arc is maintained. The lithium ion conductivity of the W-LLZO samples exhibited only a modest change after 48 h $H_2O$ exposure (Table 2). This result indicates that W-LLZO is relatively stable to $H_2O$ exposure. The morphology of the W-LLZO samples exposed to the humidified air are shown in Fig. 6. The SEM images indicate that there are almost no microstructural change and secondary phases were not observed in the W-LLZO grains and grain boundaries.

TABLE 2

Ionic conductivity of W-LLZO and $H_2O$-exposed samples for 48 h

| Conductivity ($\times 10^{-4}$ S/cm) | Air | $N_2$ | Ar |
|---|---|---|---|
| As-prepared sample | 1.09 | 2.15 | 3.13 |
| $H_2O$-exposed sample | 0.908 | 2.01 | 1.40 |

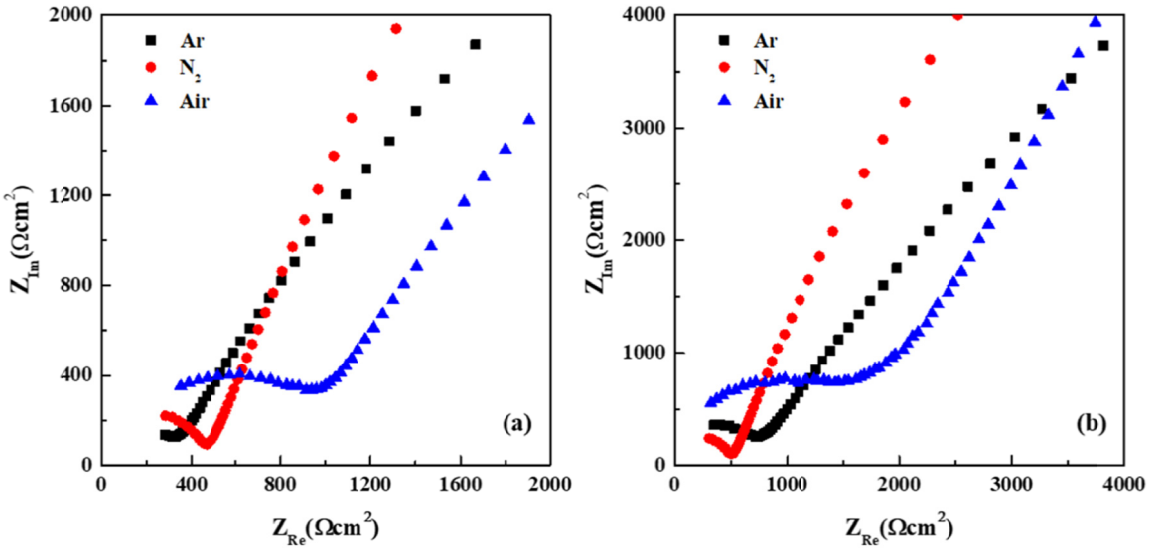


Fig. 5. AC impedance spectra of (a) as-sintered W-LLZO and (b) $H_2O$-exposed LLZO samples. Air, $N_2$, and Ar indicate sintering atmospheres

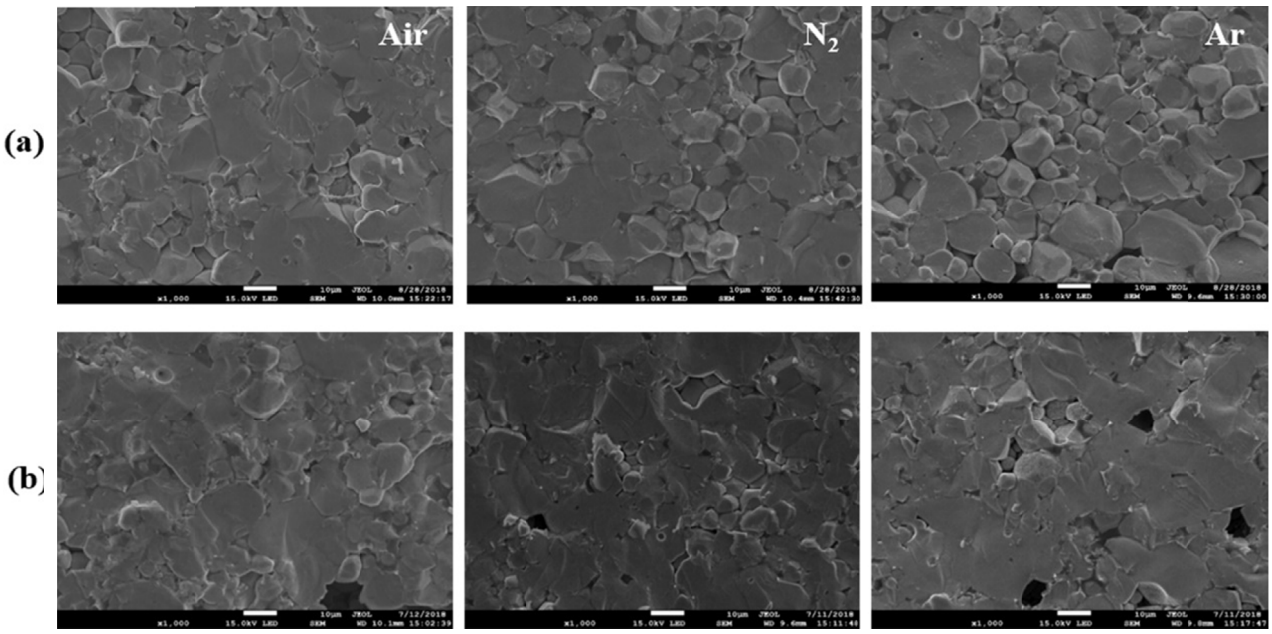


Fig. 6. SEM images of (a) as-sintered W-LLZO and (b) $H_2O$-exposed LLZO samples. Air, $N_2$, and Ar indicate sintering atmospheres

## 3. Conclusions

Al and Nb-doped and W-doped LLZO electrolyte samples were prepared by sintering LLZO powders under various atmospheres and subsequently exposed to humidified air. XRD analysis showed that the as-sintered LLZO samples were cubic phase with no secondary phases or unwanted reaction phases. After $H_2O$-exposure, a cubic to tetragonal transformation was observed in two LLZO samples, suggesting that the LLZO reacts with $H_2O$. In the case of Al and Nb-LLZO, the lithium ion conductivity decreased dramatically, while W-LLZO showed a modest decrease. These results suggest that W-LLZO is stable against water vapor. In addition, there was no significant change in the microstructure of $H_2O$-exposed W-LLZO.

### Acknowledgments

This research was supported by the Basic Science Research Program through the National Research Foundation of Korea (NRF) funded by the Ministry of Education (NRF-2016R1A2B2011517). This work was also supported by the Energy Efficiency & Resources of the Korea Institute of Energy Technology Evaluation and Planning (KETEP) grant funded by the Korea government Ministry of Knowledge Economy (No. 20172420108680).

## REFERENCES

[1] V. Etacheri, R. Marom, R. Elazari, G. Salitra, D. Aurbach, Energy Environ. Sci. **4**, 3243-3262 (2011).
[2] H. Park, S. Lee, M. Jo, S. Park, K. Kwon, M.K. Shobana, H. Choe, J. Korean Ceram. Soc. **54** (5), 438-442 (2017).
[3] J.H. Kim, D.K. Kim, J. Korean Ceram. Soc. **55** (4), 307-324 (2018).
[4] J.W. Fergus, J. Power Sources **195**, 4554-4569 (2010).
[5] E. Quartarone, P. Mustarelli, Chem. Soc. Rev. **40**, 2525-2540 (2010)
[6] M. Catti, Chem. Mater. **19**, 3963-3972 (2007).
[7] C. Uhlmann, P. Braun, J. Illig, A. Weber, E. Ivers-Tiffée, J. Power Sources **307**, 578-586 (2016).
[8] N. Anantharamulu, K.K. Rao, G. Rambabu, B.V. Kumar, V. Radha, M. Vithal, J. Mater. Sci. **46**, 2821-2837 (2011).
[9] S.Y. Lim, H. Kim, R.A. Shakoor, Y. Jung, J.W. Choi, J. Electrochem. Soc. **159**, A1393-A1397 (2012).
[10] M. Tatsumisago, M. Nagao, A. Hayashi, J. Asian Ceram. Soc. **1**, 17-25 (2013).
[11] T. Thompson, J. Wolfenstine, J.L. Allen, M. Johannes, A. Huq, I.N. David, J. Sakamoto, J. Mater. Chem. A **2**, 13431-13436 (2014).
[12] S.A. Yoon, N.R. Oh, A.R. Yoo, H.G. Lee, H. C. Lee, J. Korean Ceram. Soc. **54** (4), 278-284 (2017).
[13] C.E. Kim, H.C. Hwang, M.Y. Yoon, B.H. Choi, H.J. Hwang, J. Non-Cryst. Solids **357**, 2863-2867 (2011).
[14] N.J. Dudney, J. Power Sources **89**, 176-179 (2000).
[15] N.J. Dudney, J. Nanda, W. West, Handbook of Solid-State Batteries and Capacitors: Chapter, Superionic conducting oxide electrolytes, World Scientific 2014.
[16] Y. Jin, P.J. McGinn, Electrochim. Acta **89**, 407-412 (2013).
[17] W. Xia, B. Xu, H. Duan, Y. Guo, H. Kang, H. Li, H. Liu, ACS Appl. Mater. Interfaces **8**, 5335-5342 (2016).
[18] L. Cheng, E.J. Crumlin, W. Chen, R. Qiao, H. Hou, S.F. Lux, V. Zorba, R. Russo, R. Kostecki, Z. Liu, K. Persson, W. Yang, J. Cabana, T. Richardson, G. Chen, M. Doeff, Phys. Chem. Chem. Phys. **16**, 18294-18300 (2014).
[19] W. Xia, B. Xu, H. Duan, Xi. Tang, Y. Guo, H. Kang, H. Li, H. Liu, J. Am. Ceram. Soc. **100**, 2832-2839 (2017).
[20] Y. Jin, P.J. McGinn, J. Power Sources **239**, 326-331, (2013).
[21] I. Kokal, M. Somer, P.H.L. Notten, H.T. Hintzen, Solid State Ionics **185**, 42-46 (2011).